Chemical Science

ROYAL SOCIETY OF CHEMISTRY

EDGE ARTICLE

View Article Online
View Journal | View Issue

Cite this: *Chem. Sci.*, 2020, **11**, 5339

All publication charges for this article have been paid for by the Royal Society of Chemistry

Observation of binding of carbon dioxide to nitro-decorated metal–organic frameworks†‡

Thien D. Duong,[a] Sergey A. Sapchenko,[abc] Ivan da Silva,[d] Harry G. W. Godfrey,[a] Yongqiang Cheng,[e] Luke L. Daemen,[e] Pascal Manuel,[d] Mark D. Frogley,[f] Gianfelice Cinque,[f] Anibal J. Ramirez-Cuesta,[e] Sihai Yang *[a] and Martin Schröder *[a]

Received 25th August 2019
Accepted 26th February 2020

DOI: 10.1039/c9sc04294f

rsc.li/chemical-science

Metal–organic frameworks (MOFs) functionalised with amine, amide and hydroxyl groups show great promise for CO_2 binding due to their ability to form hydrogen bonds to CO_2. Herein we report the adsorption and selectivity of CO_2 in four iso-reticular MOFs adopting the NbO topology. Functionalisation of the parent MOF, MFM-102, with $-NO_2$, $-NH_2$ and alkyl groups leads to an enhancement of CO_2 adsorption of up to 36% for the NO_2-decorated MOF and with raised selectivity. MFM-102-NO_2 shows the highest adsorption capacity for CO_2 (184 $cm^3\ g^{-1}$ at 273 K and 1.0 bar) within this series, comparable to the best-behaving iso-reticular MOFs. At 298 K and 1.0 bar, MFM-102-NO_2 shows a CO_2/CH_4 selectivity of 5.0. *In situ* inelastic neutron scattering and synchrotron FT-IR micro-spectroscopy were employed to elucidate the host–guest interaction dynamics within CO_2-loaded MFM-102-NO_2. Neutron powder diffraction enabled the direct observation of the preferred binding domains in MFM-102-NO_2, and, to the best of our knowledge, we report the first example of CO_2 binding to a $-NO_2$ group in a porous MOF. Synergistic effects between the $-NO_2$ group and the open metal sites lead to optimal binding of CO_2 molecules within MFM-102-NO_2 *via* hydrogen bonding to C–H groups.

Introduction

Emissions of carbon dioxide (CO_2) are causing significant environmental impacts.[1] However, CO_2 is also an inexpensive, non-toxic and a potentially abundant renewable C_1 source, and, therefore, the development of cost-effective and efficient methods for carbon capture and storage (CCS) is a major target. State-of-the-art CCS is often based upon scrubbing systems that rely heavily upon the use of toxic and corrosive amines, and require high operational cost. In contrast, reversible physisorption of CO_2 within porous materials is a promising approach with the potential of low running-cost and high efficiency. A wide spectrum of materials, such as zeolites, activated carbons, ionic liquids and silica-based materials have been investigated for CO_2 adsorption.[2–5]

Metal–organic framework (MOF) materials show potential for gas adsorption and storage owing to their high porosity and designed pore size and structure reflecting their versatility *via* incorporation of active binding sites by decoration of the pores with functional groups and/or by incorporation of open metal sites.[6,7] MOFs decorated with $-NH_2$,[8] –OH,[9] –CONH–,[10] piperazine,[11] and pyridyl groups[12] have been explored extensively for CO_2 adsorption. The nitro group ($-NO_2$) is one of the most powerful electron-withdrawing groups, which can polarise –CH groups on phenyl rings. We argued that potentially this might lead to enhanced interactions between –CH groups and adsorbed CO_2 molecules, and moreover, the $-NO_2$ group might itself serve as a binding site for CO_2 molecules *via* dipole/quadrupole interactions.[13,14] However, to date, experimental evidence of CO_2 binding to NO_2-decorated MOFs has not been reported. Herein, we report the adsorption and selectivity of CO_2 in four iso-reticular NbO-type MOFs with different organic functional groups, namely $-NO_2$, $-NH_2$ and alkyl groups. The introduction of these functional groups inevitably reduces the pore volume of the parent MOF, but leads to notable enhancement in CO_2

[a]*School of Chemistry, University of Manchester, Manchester, M13 9PL, UK. E-mail: Sihai.Yang@manchester.ac.uk; M.Schroder@manchester.ac.uk*

[b]*Nikolaev Institute of Inorganic Chemistry, Siberian Branch of the Russian Academy of Sciences, 3, Acad. Lavrentieva Ave., Novosibirsk, 630090, Russia*

[c]*Faculty of Natural Sciences, Novosibirsk State University, 2, Pirogova St., Novosibirsk, 630090, Russia*

[d]*ISIS Facility, STFC Rutherford Appleton Laboratory, Chilton, Oxfordshire, OX11 0QX, UK*

[e]*Oak Ridge National Laboratory, Oak Ridge, TN 37831, USA*

[f]*Diamond Light Source, Harwell Science and Innovation Campus, Oxfordshire, UK*

† Electronic supplementary information (ESI) available: Synthetic procedures, characterization and additional analysis of crystal structures. Single crystal data of CO_2-loaded MFM-102-NO_2 is deposited at Cambridge Crystallographic Data Centre (CCDC) 1860478. For ESI and crystallographic data in CIF or other electronic format see DOI: 10.1039/c9sc04294f

‡ The crystal data for MFM-102-NO_2, MFM-102-NH_2, and bare MFM-102-NO_2, CCDC 1857304, 1857305 and 1857873, respectively, were previously reported in ref. 16.

adsorption. In particular, the NO_2-functionalised MOF MFM-102-NO_2 shows a 36% increase in CO_2 uptake compared to the parent MFM-102, confirming a positive effect on CO_2 binding. A combination of static and dynamic experiments using *in situ* neutron powder diffraction (NPD), inelastic neutron scattering (INS) and synchrotron-based IR micro-spectroscopy have been applied to study the binding domains of adsorbed CO_2 and the host–guest binding dynamics in MFM-102-NO_2 as a function of CO_2 loading to reveal fundamental insights into the mechanisms for enhanced CO_2 adsorption.[15]

Experimental

Material and instrumentation

Chemicals and reagents were purchased from Fisher Scientific, Sigma Aldrich or Fluorochem and used as received without further purification. The detailed synthesis of MFM-102 has been reported previously.[16] ^{1}H NMR and ^{13}C NMR spectra were measured on a Bruker AV400 or AV500 spectrometer. High-resolution electrospray mass spectra were measured on a Bruker MicroTOF spectrometer with samples dissolved in MeOH, and scanning was conducted in both positive and negative modes. Infrared (IR) spectra were recorded in the 400–4000 cm^{-1} range in ATR sampling mode with a Thermo Scientific iD5 diamond ATR on a Nicolet iS5 FT-IR spectrometer, and elemental analysis was carried out on a CE-440 elemental analyser (EAI Company). TGA measurements were performed using a PerkinElmer TGA 7 Gravimetric Analyser under a flow of N_2 (20 ml min^{-1}) at a heating rate of 5 °C min^{-1}. Powder X-ray diffraction (PXRD) patterns were obtained on a PANalytical X'Pert Pro MPD diffractometer in Bragg–Brentano geometry with Cu-$K_{\alpha 1}$ radiation ($\lambda = 1.5406$ Å) at 40 kV and 30 mA over 2θ range 3–40°. Samples were evenly dispersed on zero-background silicon plates with a cavity depth of 0.3 mm.

Neutron powder diffraction (NPD) of gas-loaded MFM-102-NO_2

NPD data were collected at WISH beamline at ISIS Muon and Neutron facility. Acetone exchanged MFM-102-NO_2 was loaded into vanadium cans of 11 mm diameter, and the sample was activated by heating at 393 K and at 1×10^{-7} mbar for 2 days. Data for the bare framework were collected after placing the sample can into a liquid He cryostat and cooling to 7 K. CO_2 gas was dosed into the system after warming to 290 K. The gases were dosed volumetrically from a calibrated volume, and to ensure gases were fully adsorbed into the sample without condensation elsewhere the system was cooled to 7 K slowly over 3 h. Structure solutions of gas-loaded MFM-102-NO_2 were solved by sequential difference Fourier analyses followed by Rietveld refinements (see ESI† Section 4).

Inelastic neutron scattering (INS) of CO_2-loaded MFM-102-NO_2 and MFM-102-NH_2

INS data were collected on the TOSCA beamline at ISIS Muon and Neutron facility and on the VISION spectrometer at Spallation Neutron Source, Oak Ridge National Laboratory (USA). MFM-102-NO_2 and MFM-102-NH_2 were loaded into a vanadium can of 11 mm diameter and outgassed at 10^{-7} mbar at 393 K for 2 days. After placing the sample into a He cooled cryostat, INS data of the bare framework were collected at 7 K. CO_2 was dosed volumetrically from a calibrated volume at room temperature and gradually cooled to 7 K to allow the gas to fully adsorb into MFM-102-NO_2 and MFM-102-NH_2. INS data of CO_2-loaded MFM-102-NO_2 and CO_2-loaded MFM-102-NH_2 were collected at 7 K. Experimentally obtained INS data were compared with modelled data obtained *via* density functional theory (DFT) calculations (see ESI† for further details).

Synchrotron FTIR micro-spectroscopy of CO_2-loaded MFM-102-NO_2

Single crystals of MFM-102-NO_2 were loaded onto a ZnSe slide and placed into a Linkam FTIR600 variable temperature gas-tight cell fitted with ZnSe windows. The MOF sample was activated *in situ* under a flow of N_2 whilst heating the Linkam stage to 413 K for 6 h. Partial pressures of zeolite dried gases N_2 and CO_2 were controlled by varying the volumetric flow of the two gases *via* separate mass flow controllers. FTIR spectra were collected at B22 MIRIAM beamline at Diamond Light Source using a highly bright synchrotron IR source connected to a Bruker Hyperion 3000 IR microscope with a 15× objective and MCT detector (liq. N_2 cooled). Spectra (256 scans) were measured at room temperature with a 20 × 20 μm beam, in the spectral range of 4000–650 cm^{-1} (4 cm^{-1} resolution).

Results and discussion

Synthesis, structure and porosity

MFM-102, MFM-102-NH_2, MFM-102-NO_2 and MFM-111 were synthesised according to our previously reported methods,[16–18] and the phase purity of all bulk materials was confirmed by powder X-ray diffraction (see ESI† Section 1). All four MOFs are iso-structural and crystallise in the trigonal space group $R\bar{3}m$. The framework is built from $Cu_2(O_2CR)_4$ paddlewheel units in which two Cu^{II} cations are bridged by four carboxylate groups surrounded the [Cu···Cu] axis and two terminal H_2O molecules at axial positions to form a $[Cu_2(O_2CR)_4(OH_2)_2]$ node. These $Cu_2(O_2CR)_4$ units are bridged by the diisophthalate ligands to afford a 3D extended NbO-type network. Within each framework, there are two different types of metal–ligand cages (denoted as A and B) in a 1 : 1 ratio (Fig. 1). Cage A consists of six $Cu_2(O_2CR)_4$ paddlewheels and six linkers to give a spherical shape of 15 Å diameter. Cage B is constructed of twelve $Cu_2(O_2CR)_4$ paddlewheels residing at the vertices and six ligands on the faces to form an ellipsoid shaped cavity of 32 Å along the *c* axis and 18 Å across *ab* plane. Due to the alternative packing of cages A and B, the alkyl, nitro, and amino groups are directly grafted into the pore walls, providing an excellent platform to study their role in guest binding. The Brunauer–Emmett–Teller (BET) surface area and pore volume of MFM-102, MFM-111, MFM-102-NH_2, MFM-102-NO_2 were determined to be 3412, 2930, 2928, 2893 m^2 g^{-1} and 1.29, 1.19, 1.12, 1.14 cm^3 g^{-1}, respectively, from N_2 isotherms at 77 K. As

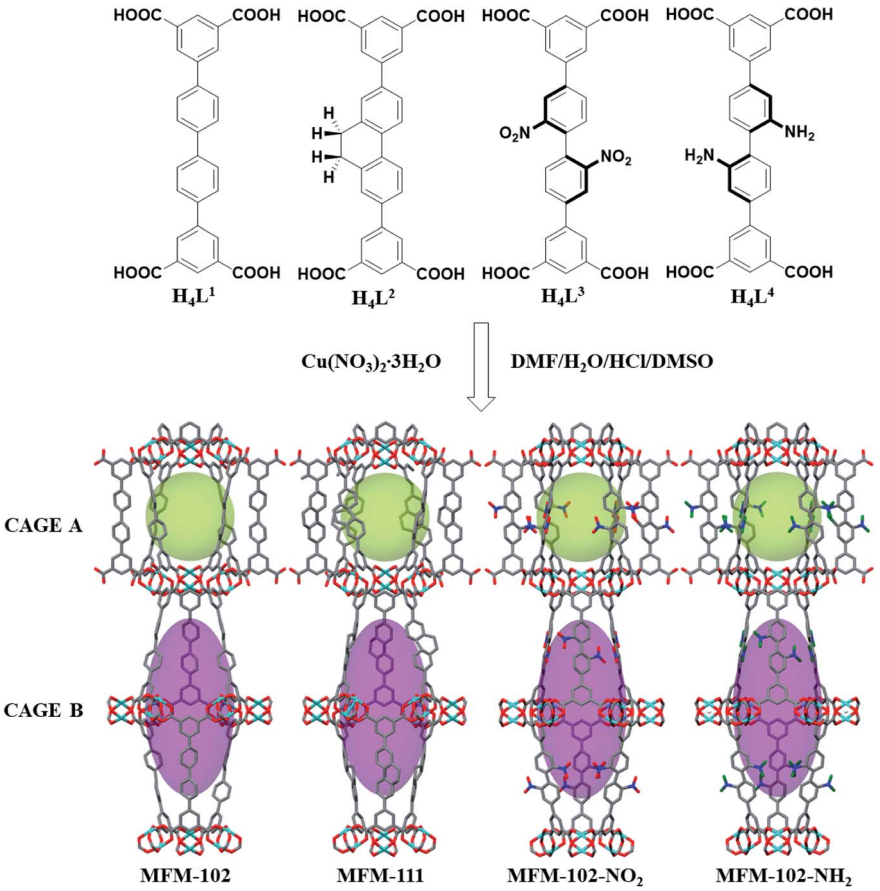

Fig. 1 Views of organic ligands used to construct the MFM-102 series of MOFs and the X-ray crystal structures of MFM-102, MFM-111, MFM-102-NO_2 and MFM-102-NH_2. The functional groups are highlighted in ball-stick mode. (C, dark grey; O, red; N, blue; Cu, turquoise; all coordinated H_2O and hydrogen atoms are omitted for clarity, except for the hydrogen atoms on the $-NH_2$ group, green).

expected, the porosity of decorated complexes reduces compared to the parent MOF, and so introduction of alkyl, $-NH_2$ and $-NO_2$ groups into MFM-102 leads to reduction in BET surface areas of 14%, 14% and 15%, respectively.

Gas adsorption properties

Adsorption isotherms of CO_2 and CH_4 were recorded at 273 and 298 K up to 1 bar. All isotherms are completely reversible, and show fast adsorption–desorption kinetics with equilibrium achieved typically within 3–5 min. Uptake of CO_2 at 273 K and 1.0 bar were recorded as 184, 178, 165, 135 $cm^3\ g^{-1}$ for MFM-102-NO_2, MFM-102-NH_2, MFM-111 and MFM-102, respectively (Fig. 2a). Interestingly, despite the reduction in porosity, the introduction of alkyl, $-NH_2$ and $-NO_2$ groups into MFM-102 leads to enhancement on the CO_2 uptake of resultant MOFs by 22%, 32% and 36%, respectively. Notably, the CO_2 uptake of MFM-102-NO_2 is comparable to the best-performing isoreticular MOF (NJU-Bai-14, 187 $cm^3\ g^{-1}$) under the same conditions.[19] Similar enhancement of CO_2 adsorption was also observed at 298 K for the decorated MOFs (Fig. 2b), and these uptakes are comparable to other leading NbO-type MOFs (Table 1). In sharp contrast, these MOFs show similarly low uptakes of CH_4 at 273 and 298 K and 1.0 bar (ranging from 30 $cm^3\ g^{-1}$ to 20 $cm^3\ g^{-1}$). This result indicates the potential of MFM-102-NO_2 as a promising material for selective adsorption of CO_2. The adsorption selectivities for equimolar mixtures of CO_2/CH_4 within these MOFs have been calculated using ideal adsorbed solution theory (IAST) using the experimental single–component isotherm data (Fig. S4 and S5†). At 298 K and 1 bar, the CO_2/CH_4 (50 : 50) selectivity is 5.0, which is comparable to those reported for other Cu-based MOFs with similar porosity, such as NJU-Bai12 (5.0),[20] ZJNU-81(5.5),[21] ZJNU-82 (5.4),[21] ZJNU-83 (4.9),[21] ZJU-15 (4.4) (ref. 22) and ZJNU-57 (5.5),[23] but which do not show NbO topologies.

The isosteric heats of adsorption (Q_{st}) of CO_2 were calculated using virial method based on isotherm data at 273 and 298 K (Fig. 2c). The values for Q_{st} at low surface coverage range from 24.0 to 24.6 kJ mol^{-1}, comparable to other MOFs of NbO topology with a high density of open Cu(II) sites (Table 1). With increasing CO_2 loading, the values of Q_{st} steadily reduce in all four cases. Interestingly, the Q_{st} values of MFM-102 drop more rapidly than functionalised materials with increasing loading, indicating the presence of additional binding sites in the decorated MOFs.

In situ neutron powder diffraction (NPD) of CO_2-loaded MFM-102-NO_2

In situ NPD was employed to determine the binding domains for adsorbed CO_2 molecules within desolvated MFM-102-NO_2 at

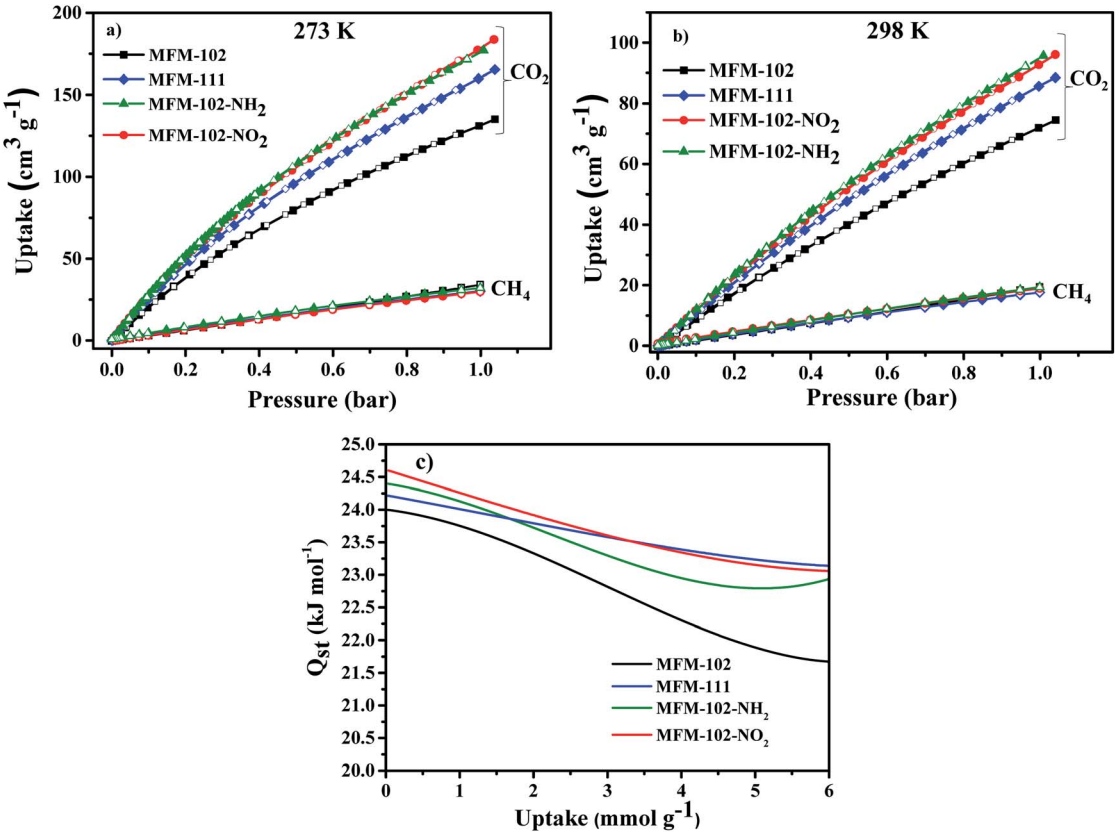

Fig. 2 Adsorption isotherms for desolvated MFM-102, MFM-111, MFM-102-NO_2 and MFM-102-NH_2 (a) 273 K, (b) 298 K. Solid and open symbols represent adsorption and desorption, respectively. (c) Heat of adsorption as a function of CO_2 uptake derived by the virial method.

a loading of 2.0 CO_2/Cu. NPD data for the desolvated complex confirm the complete removal of guest solvents, including coordinated H_2O molecules on the Cu sites, and no significant structural distortion is observed compared to the parent solvated material. A loading of 2.0 CO_2/Cu was used to assess the strongest binding sites within the material without involving notable adsorbate–adsorbate interactions. Fourier difference map analysis of the NPD patterns afforded the location of guest CO_2 molecules, which after further development by Rietveld refinement, allowed unambiguous determination of gas positions, orientations and crystallographic occupancies within each sample.

MFM-102-NO_2 displays six binding sites for CO_2 (denoted as I to VI with decreasing occupancies, Fig. 3 and 4). Significantly, site I (occupancy = 0.50) was found not to be at the open Cu(II) sites but is confined to the window between Cages A and B. At site I, CO_2^{I} forms supramolecular interactions to aromatic –CH group from two adjacent NO_2-substituted phenyl rings [$O_{CO_2}\cdots$HC– = 2.13(5), 2.42(8) Å]. It is noteworthy that –NO_2 is a strong electron-withdrawing groups which leads to

Table 1 Comparison of CO_2 uptakes in selected Cu-MOFs of NbO topology

MOFs	CO_2 uptake, 273 K ($cm^3\ g^{-1}$)	CO_2 uptake, 298 K ($cm^3\ g^{-1}$)	V_p, pore volume ($cm^3\ g^{-1}$)	BET area ($m^2\ g^{-1}$)	Q_{st} (kJ mol^{-1})	Ref.
ZJNU-44	175	116	0.894	2314	—	24
ZJNU-43	180	103	0.894	2243	—	24
ZJNU-45	163	107	0.877	2232	—	24
ZJNU-40	—	86	0.997	2072	24.0	25
ZJNU-41	—	97	0.837	2530	23.5	26
ZJU-8	175	98	1.022	2501	21.9	27
NJU-Bai-14	187	100	0.942	2384	24.5	19
MFM-101	164	86	1.080	2805	—	25
MFM-102	135	74	1.297	3412	24.0	This work
MFM-102-NO_2	184	96	1.118	2893	24.6	This work
MFM-102-NH_2	180	97	1.140	2928	24.4	This work
MFM-111	165	88	1.190	2930	24.2	This work
MFM-130	109	59	1.000	2173	26.0	28

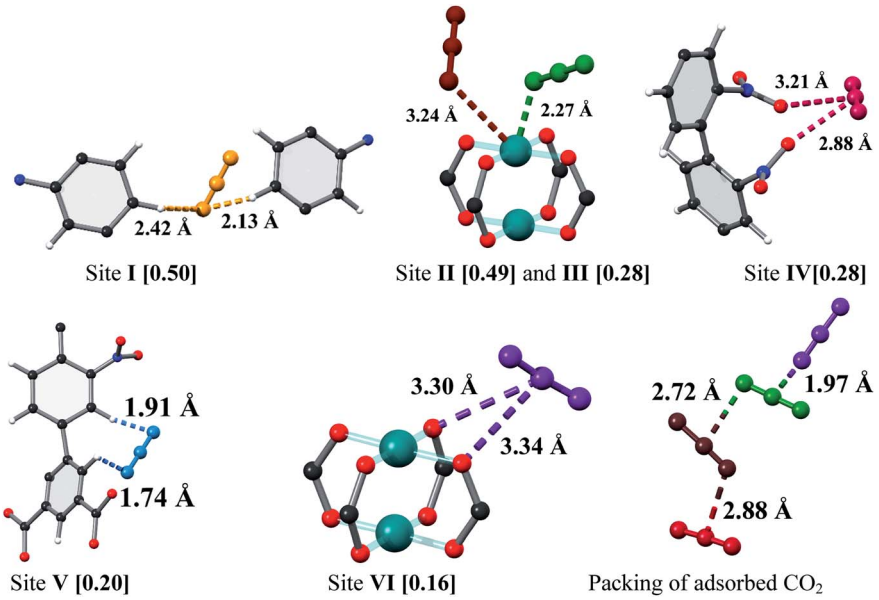

Fig. 3 View of the binding sites for adsorbed CO_2 molecules in MFM-102-NO_2 and the relative positions of these positions in the framework cages [C, dark grey; O, red; N, blue; Cu, turquoise and CO_2 molecules at site I (yellow), site II (green), site III (brown), site IV (ruby), site V (blue) and site VI (purple)].

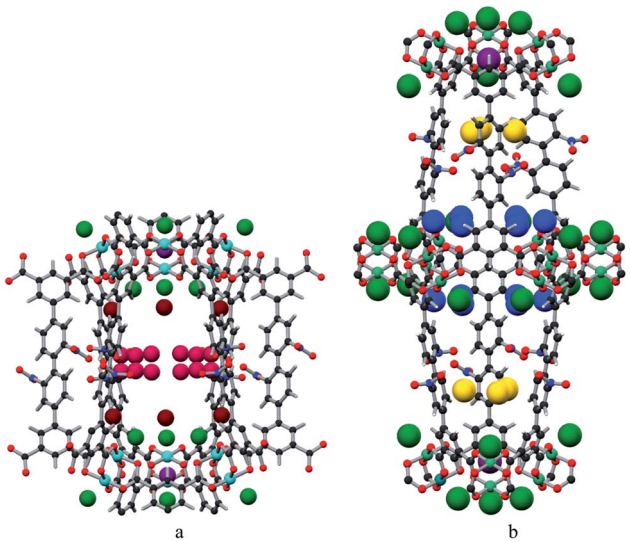

Fig. 4 The positions of the CO_2 in the framework cage A (a) and B (b) of MFM-102-NO_2. CO_2 molecules are at site I (yellow), site II (green), site III (brown), site IV (ruby), site V (blue) and site VI (purple).

polarisation of adjacent –CH moieties. These –CH groups therefore show enhanced acidity and thus act as effective hydrogen bond donors to CO_2 molecules. Site II and III (occupancy = 0.49 and 0.28, respectively) reside at the open Cu(II) centre [$O_{CO_2}\cdots$Cu = 2.27(7) Å and 3.24(7) Å for site II and III, respectively]. Site IV (occupancy = 0.28) is stabilised by the dipole/quadrupole interaction between O(δ^-) of the –NO_2 group from 2 neighbouring phenyl rings and the C(δ^+) centre of CO_2 with distances of 3.20(6) and 2.87(9) Å. Site V (occupancy = 0.20) was found close to the isophthalate phenyl ring [$O_{CO_2}\cdots$HC– = 1.72(9) Å] and the NO_2-decorated phenyl ring [$O_{CO_2}\cdots$HC– = 1.91(4) Å] stabilised by interactions with aromatic hydrogen atoms. At site VI (occupancy = 0.167), the C atom of CO_2 is close to the two oxygen atoms from carboxylate groups of the [$Cu_2(O_2CR)_4$] paddlewheel with distances of 3.30(1)–3.34(5) Å. Overall, the effects of –NO_2 groups on CO_2 binding are two-fold: (i) polarising neighbouring phenyl C–H bonds *via* the conjugate effect of the aromatic ring bound to electron-withdrawing –NO_2 groups (site I), and (ii) creating additional adsorption sites *via* direct dipole/quadrupole interaction of –NO_2 with CO_2 (site IV).

In situ synchrotron FT-IR micro-spectroscopy of MFM-102-NO_2

To investigate further the nature of host–guest interactions, *in situ* synchrotron FT-IR micro-spectroscopy was conducted on a single crystal of activated MFM-102-NO_2. FTIR spectra were collected as a function of CO_2-loading by increasing the partial pressure of CO_2 in N_2 from 0 to 1.0 bar ($ppCO_2$) (Fig. 5a). Gaseous CO_2 has three fundamental vibrational modes: the symmetric C=O stretching mode ν_1 (1388 cm^{-1}), a doubly-generate bending mode ν_2 (667 cm^{-1}) and an asymmetric stretching vibration ν_3 (2349 cm^{-1}) (Table S1†).[29] The $\nu_1 + \nu_3$ (3714 cm^{-1}) and $2\nu_2 + \nu_3$ (3612 cm^{-1}) combination bands of CO_2 (Fig. 5a) were used to monitor CO_2 sorption as the fundamental anti-symmetric stretch at ~2348 cm^{-1} saturates at $ppCO_2$ above 0.2 bar. On adsorption, a combination of electrostatic and dispersion forces between CO_2 and the pore surface weakens the C=O bonds in CO_2, leading to the observed redshift of IR bands of adsorbed CO_2 to lower frequencies (3700 and 3600 cm^{-1}, respectively) compared to those observed in gas phase (Table S1†). If CO_2 strongly coordinates to an open metal

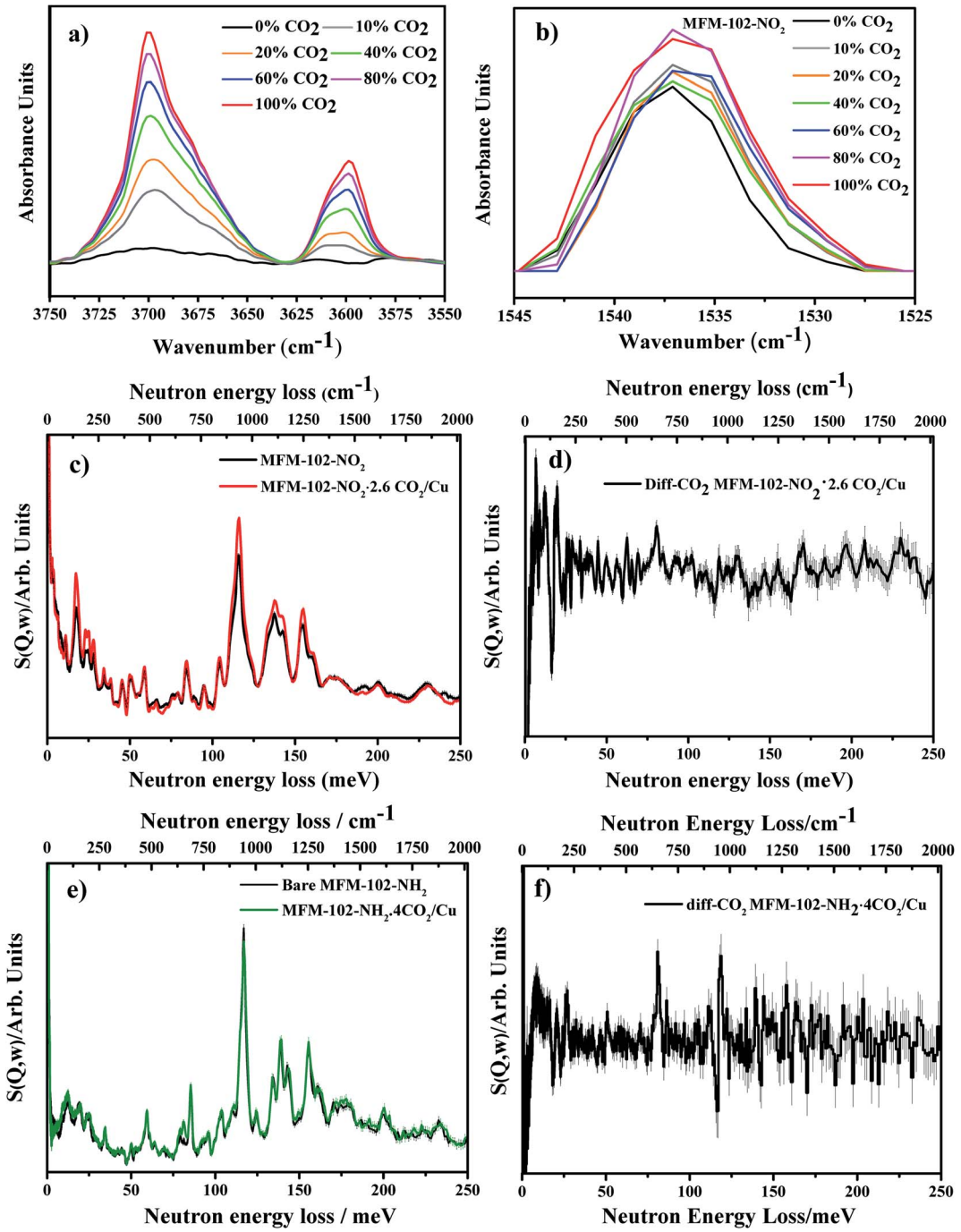

Fig. 5 (a) IR spectra showing the adsorption of CO_2 into MFM-102-NO_2 and demonstrating the growth in $\nu_1 + \nu_3$ and $2\nu_2 + \nu_3$ combination bands for CO_2 near 3700 cm^{-1} and 3600 cm^{-1}. (b) Changes in intensity and broadening of the N=O asymmetric stretching vibration with CO_2 loading. (c) INS spectra for activated MFM-102-NO2 and MFM-102-NO_2 with CO_2 loading. (d) Difference INS plot, derived by subtracting INS spectra for CO_2-loaded MFM-102-NO_2 and bare MFM-102-NO_2 spectra. (e) and (f) are the same as (c) and (d), respectively, but replacing MFM-102-NO_2 with MFM-102-NH_2.

site, the molecular symmetry is lowered and the degeneracy of the ν_2 bending mode is removed, splitting the band into two peaks.[30] Three IR spectra of the activated, 10% CO_2- and 100% CO_2-loaded MFM-102-NO_2 reveal the changes in the peak at 660 cm^{-1}. This peak shows a significant increase in intensity at 10% CO_2 loading, and broadens and splits into two peaks at 657 cm^{-1} and 663 cm^{-1} at 100% CO_2 loading (Fig. S7a†). The IR band of the host framework reveals some interesting features. There is a continuous red shift of the band at 1670 cm^{-1} (the C=O stretching mode of –COO groups[31]) with increasing CO_2 loading, consistent with the interactions between CO_2 molecules and $[Cu_2(O_2CR)_4]$ paddlewheel units (site VI, Fig. S7b†). An

apparent change in the peak shape and intensity at 1537 cm^{-1} (N–O asymmetric stretching mode in the $–NO_2$ group[32]) suggests dipole/quadrupole interaction between the $–NO_2$ groups and adsorbed CO_2 molecules (Fig. 5b). In the low energy regions, the peak at 1025 cm^{-1} (corresponding to C–H out-of-plane wagging[33]) gradually decreases in intensity with increasing CO_2 loading, while the peak at 1005 cm^{-1} grows and shifts to lower energy (Fig. S7c†). These changes in FTIR spectra are in excellent agreement with the presence of multiple interactions between the framework and CO_2 molecules as observed by the NPD experiment.

Inelastic neutron scattering (INS) studies of CO_2-loaded MFM-102-NO_2 and MFM-102-NH_2

To gain further insight into the host–guest dynamics of CO_2-loaded MFM-102-NO_2, *in situ* INS has been investigated. The calculated INS spectrum of bare MOF was found to be in good agreement with the experimental INS data (Fig. S8†) leading to assignment of all the vibrational modes. In the INS spectrum of CO_2-loaded MFM-102-NO_2, all the INS peaks shift slightly to higher energy, attributed to a stiffening effect of the host–guest lattice on CO_2 adsorption (Fig. 4c). There are changes in the peak intensity at 164 and 193 meV, corresponding to the symmetrical and asymmetrical stretching of $–NO_2$ groups. The various distortion motions of the phenyl rings (83 meV), out-of-plane C–H bending on the isophthalate rings (116 meV) and in-plane C–H bending on phenyl rings (136 meV) increase in intensity. These results confirm the important role of $–NO_2$ and –CH groups on the adsorption of CO_2. Similarly, the difference INS spectra of CO_2-adsorbed MFM-102-NH_2 also show changes in intensity of the peaks at 80, 117, 119 meV, originating from various in-plane deformational vibrations of the phenyl rings and the wagging motion of aromatic C–H groups. These changes are attributed to the reduction of the motion of aromatic C–H groups with the introduction of CO_2 into the framework.

Conclusions

We report a comprehensive investigation of the adsorption and binding of CO_2 in four iso-reticular MOFs with varying functional groups. Introduction of $–NO_2$ group to the parent MOF, MFM-102, leads a 15% reduction on the BET surface area but a 36% enhancement on the CO_2 adsorption capacity at 273 K and 1.0 bar. NPD analysis of CO_2-loaded MFM-102-NO_2 reveals cooperative binding of CO_2 to –CH hydrogen bond donors that is enhanced by the electron withdrawing effects of the $–NO_2$ groups that decorate pore walls. In addition, direct interaction of CO_2 with the open metal sites and the $–NO_2$ groups is observed, thus enhancing further interaction of the MOF with CO_2. The *in situ* spectroscopic studies using INS and FTIR spectroscopy establish that adsorbed CO_2 molecules interact strongly with the $–NO_2$ and –CH groups of MFM-102-NO_2, with apparent shifts and changes of intensity of N=O and C–H vibrational bands on CO_2 loading. This work provides a fundamental understanding of the effect of the $–NO_2$ group on CO_2 adsorption, and the information gained here provides further insights into the development of materials showing improved gas binding *via* specific interaction with ligand sites within the MOF structure.

Conflicts of Interest

The authors declare no competing interests.

Acknowledgements

We thank EPSRC (EP/I011870), the Royal Society and University of Manchester for funding. This project has received funding from the European Research Council (ERC) under the European Union's Horizon 2020 research and innovation programme (grant agreement no 742401, NANOCHEM). We thank ISIS/STFC, Diamond Light Source and Oak Ridge National Laboratory for access to Beamlines WISH, B22 and VISION, respectively. Neutron scattering experiments were performed at ORNL's Spallation Neutron Source, supported by the Scientific User Facilities Division, Office of Basic Energy Sciences, US DOE, under Contract No. DE-AC0500OR22725 with UT Battelle, LLC. The computing resources were made available through the VirtuES and the ICE-MAN projects, funded by Laboratory Directed Research and Development program and Compute and Data Environment for Science (CADES) at ORNL.

Notes and references

1 D. W. Keith, *Science*, 2009, **325**, 1654–1655.
2 E. David and J. Kopac, *J. Anal. Appl. Pyrolysis*, 2014, **110**, 322–332.
3 T. D. Pham, R. Xiong, S. I. Sandler and R. F. Lobo, *Microporous Mesoporous Mater.*, 2014, **185**, 157–166.
4 M. Yang, Y. Song, L. Jiang, X. Wang, W. Liu, Y. Zhao, Y. Liu and S. Wang, *J. Ind. Eng. Chem.*, 2014, **20**, 322–330.
5 M. Ramdin, T. W. de Loos and T. J. H. Vlugt, *Ind. Eng. Chem. Res.*, 2012, **51**, 8149–8177.
6 S. Kazemi and V. Safarifard, *Polyhedron*, 2018, **154**, 236–251.
7 Y. Liao, L. Zhang, M. H. Weston, W. Morris, J. T. Hupp and O. K. Farha, *Chem. Commun.*, 2017, **53**, 9376–9379.
8 A. Greenaway, B. Gonzalez-Santiago, P. M. Donaldson, M. D. Frogley, G. Cinque, J. Sotelo, S. Moggach, E. Shiko, S. Brandani, R. F. Howe and P. A. Wright, *Angew. Chem., Int. Ed.*, 2014, **53**, 13483–13487.
9 X. Duan, H. Wang, Z. Ji, Y. Cui, Y. Yang and G. Qian, *J. Solid State Chem.*, 2016, **241**, 152–156.
10 O. Benson, I. da Silva, S. P. Argent, R. Cabot, M. Savage, H. G. W. Godfrey, Y. Yan, S. F. Parker, P. Manuel, M. J. Lennox, T. Mitra, T. L. Easun, W. Lewis, A. J. Blake, E. Besley, S. Yang and M. Schröder, *J. Am. Chem. Soc.*, 2016, **138**, 14828–14831.
11 Q. Mu, H. Wang, L. Li, C. Wang, Y. Wang and X. Zhao, *Chem.–Asian J.*, 2015, **10**, 1864–1869.
12 Q.-Q. Dang, Y.-F. Zhan, L.-N. Duan and X.-M. Zhang, *Dalton Trans.*, 2015, **44**, 20027–20031.

13 R. Banerjee, H. Furukawa, D. Britt, C. Knobler, M. O'Keeffe and O. M. Yaghi, *J. Am. Chem. Soc.*, 2009, **131**, 3875–3877.
14 S. Biswas, T. Ahnfeldt and N. Stock, *Inorg. Chem.*, 2011, **50**, 9518–9526.
15 T. L. Easun, F. Moreau, Y. Yan, S. Yang and M. Schröder, *Chem. Soc. Rev.*, 2017, **46**, 239–274.
16 T. D. Duong, S. A. Sapchenko, I. da Silva, H. G. W. Godfrey, Y. Cheng, L. L. Daemen, P. Manuel, A. J. Ramirez-Cuesta, S. Yang and M. Schröder, *J. Am. Chem. Soc.*, 2018, **140**, 16006–16009.
17 X. Lin, I. Telepeni, A. J. Blake, A. Dailly, C. M. Brown, J. M. Simmons, M. Zoppi, G. S. Walker, K. M. Thomas, T. J. Mays, P. Hubberstey, N. R. Champness and M. Schröder, *J. Am. Chem. Soc.*, 2009, **131**, 2159–2171.
18 S. Yang, X. Lin, A. Dailly, A. J. Blake, P. Hubberstey, N. R. Champness and M. Schröder, *Chem. - Eur. J.*, 2009, **15**, 4829–4835.
19 M. Zhang, Q. Wang, Z. Lu, H. Liu, W. Liu and J. Bai, *CrystEngComm*, 2014, **16**, 6287–6290.
20 B. Zheng, R. Yun, J. Bai, Z. Lu, L. Du and Y. Li, *Inorg. Chem.*, 2013, **52**, 2823–2829.
21 M. He, Y. Wang, X. Gao, S. Li and Y. He, *Dalton Trans.*, 2018, **47**, 8983–8991.
22 X. Duan, Y. Zhou, R. Lv, B. Yu, H. Chen, Z. Ji, Y. Cui, Y. Yang and G. Qian, *J. Solid State Chem.*, 2018, **260**, 31–33.
23 Y. Wang, M. He, Z. Tian, H. Zhong, L. Zhu, Y. Zhang, X. Zhang, D.-L. Chen and Y. He, *Dalton Trans.*, 2018, **47**, 2444–2452.
24 C. Song, J. Hu, Y. Ling, Y. Feng, R. Krishna, D.-l. Chen and Y. He, *J. Mater. Chem. A*, 2015, **3**, 19417–19426.
25 C. Song, Y. He, B. Li, Y. Ling, H. Wang, Y. Feng, R. Krishna and B. Chen, *Chem. Commun.*, 2014, **50**, 12105–12108.
26 C. Song, Y. Ling, L. Jin, M. Zhang, D.-L. Chen and Y. He, *Dalton Trans.*, 2016, **45**, 190–197.
27 J. Cai, H. Wang, H. Wang, X. Duan, Z. Wang, Y. Cui, Y. Yang, B. Chen and G. Qian, *RSC Adv.*, 2015, **5**, 77417–77422.
28 Y. Yan, M. Juríček, F.-X. Coudert, N. A. Vermeulen, S. Grunder, A. Dailly, W. Lewis, A. J. Blake, J. F. Stoddart and M. Schröder, *J. Am. Chem. Soc.*, 2016, **138**, 3371–3381.
29 S. Andonova, E. Ivanova, J. Yang and K. Hadjiivanov, *J. Phys. Chem. C*, 2017, **121**, 18665–18673.
30 J. G. Vitillo, M. Savonnet, G. Ricchiardi and S. Bordiga, *ChemSusChem*, 2011, **4**, 1281–1290.
31 N. R. Dhumal, M. P. Singh, J. A. Anderson, J. Kiefer and H. J. Kim, *J. Phys. Chem. C*, 2016, **120**, 3295–3304.
32 F. X. W. Robert, M. Silverstein, D. J. Kiemle and D. L. Bryce, *Spectrometric Identification of Organic Compounds*, 8th edn, 2014.
33 F. P. Ureña, M. F. Gómez, J. J. L. González and E. M. n. Torres, *Spectrochim. Acta, Part A*, 2003, **59**, 2815–2839.